Green Chemistry

PAPER

View Article Online
View Journal | View Issue

Cite this: *Green Chem.*, 2025, **27**, 6213

Techno-economic and life cycle analysis of bio-hydrogen production using bio-based waste streams through the integration of dark fermentation and microbial electrolysis†

Arna Ganguly, Pingping Sun, * Xinyu Liu, Hernan E. Delgado, Lili Sun and Amgad Elgowainy

Hydrogen derived from bio-based sources, or biohydrogen ($bioH_2$), has the potential to reduce GHG emissions from industrial and transportation sectors, owing to the low carbon footprint and myriad applications like refinery operation, ammonia production, steel production, fuel cell, etc. To evaluate the commercialization potential of $bioH_2$ production, we modeled $bioH_2$ production and conducted techno-economic analysis (TEA) and life cycle analysis (LCA) of two facilities producing 50 metric tonnes of $bioH_2$ per day from cheese whey (CW) and solid food waste (SFW) through the integration of dark fermentation (DF) and microbial electrolysis cell (MEC) technologies. LCA results showed that CW and SFW can produce carbon-negative $bioH_2$, with emissions of −8.6 and −8.0 kg GHG kg^{-1} $bioH_2$ with carbon sequestration and renewable electricity resources, respectively, making $bioH_2$ potentially eligible for a tax credit of \$3 kg^{-1} H_2 based on provision 45 V of the U.S. Inflation Reduction Act (IRA). In this study, $bioH_2$ production treats waste streams to generate fresh water, thus, potentially can receive waste water treatment fee that varies with regions. The MEC capital cost dominates the $bioH_2$ cost, which is mainly determined by current density. With a current density of 20 A m^{-2}, the production cost for CW input varied between \$17 and \$24 kg^{-1} $bioH_2$, while that for SFW input ranged from \$29 to \$30 kg^{-1} $bioH_2$ under different operating conditions, considering the 45 V tax credit, waste water treatment fee and production revenue. If the current density increases to 100 A m^{-2}, the $bioH_2$ cost decreases to a range of \$4.0–\$6.9 for CW and \$5–\$6 for SFW scenarios. This study also shows that low-cost $bioH_2$ can be produced using CW waste stream as feedstock.

Received 8th October 2024,
Accepted 28th April 2025

DOI: 10.1039/d4gc05020g

rsc.li/greenchem

Green foundation

1. This study explores the potential of organic matter-rich biowastes, such as cheese whey and solid food waste, as feedstock to produce $bioH_2$ and CO_2 following integrated biochemical routes.
2. $BioH_2$ can be used in the transportation and industrial sectors, while CO_2 can be used in the beverage industry or can be sequestered. The study showed low-cost $bioH_2$ production, especially when cheese whey is used as the feedstock, with a low environmental footprint.
3. The material cost of the MEC stack and operating current density are key cost drivers of $bioH_2$ production costs.

Introduction

Finding a clean alternative to fossil fuels has become paramount owing to the effects of carbon dioxide (CO_2) emissions on the global climate, such as melting glaciers, rising sea levels, intense heat waves, and an increased number of wildfires.[1] Alternatives must be environmentally sustainable and commercially viable. Hydrogen (H_2) is a potential clean alternative fuel because it is a zero-carbon energy carrier that can be produced from a variety of non-fossil sources. Currently, the United States (U.S.) produces about 10 million metric tonnes (MT) of hydrogen annually, mainly for petroleum refining and ammonia production.[2–4] According to Ruth *et al.*, H_2 demand may grow to around 22–41 MMT per year, with potential uses in emerging industrial sectors and transportation applications.[5]

Hydrogen is a zero-carbon molecule, but its current production *via* steam methane reforming (SMR) of natural gas is carbon intensive. The life cycle greenhouse gas (GHG) emis-

Energy Systems and Infrastructure Assessment Division, Argonne National Laboratory, 9700 S. Cass Avenue, Lemont, IL 60439, USA. E-mail: psun@anl.gov

† Electronic supplementary information (ESI) available. See DOI: https://doi.org/10.1039/d4gc05020g

sions of SMR hydrogen are approximately 10 kilograms (kg) of CO_2 equivalent (CO_{2e}) per kg H_2 produced.[6] Clean hydrogen can be produced *via* water electrolysis using renewable or nuclear electricity, leading to near-zero fuel cycles or well-to-wheel (WTW) GHG emissions (*i.e.*, excluding equipment-embodied emissions). However, the electrolysis of water consumes a significant amount of electricity, ranging from 40 to 55 kW h kg^{-1} H_2,[7] depending on the technology employed.

This work investigates an alternative clean hydrogen production technology that produces bio-hydrogen from waste streams using the integration of dark fermentation and microbial electrolysis cells (DF-MECs).

Wastewater is an abundant resource in today's urbanized world. According to the U.S. Department of Energy (DOE), wastewater treatment consumes around 30 terawatt-hours of electricity per year in the U.S., leading to an annual cost of approximately $2 billion. Wastewater contains a significant amount of energy in the form of organic compounds (or contaminants), which, if captured, can be transformed into valuable products, including H_2.[8] Shen *et al.*[9] reported that 86% of wastewater treatment plants (WWTPs) with an average wastewater flow rate of 10–100 million gallons per day with anaerobic digestion systems utilize biogas, out of which around 5% are upgraded to pipeline renewable natural gas (RNG). Further research is required to overcome technical barriers, such as biogas upgrading and cleanup. An alternative pathway for waste energy utilization is recovery as bioH_2. With the market price of H_2 at $1.50 kg^{-1} or $13 $MMBtu^{-1}$ H_2,[10] it has a higher market value than RNG (assuming the market price of natural gas to be $4 $MMBtu^{-1}$ (ref. 11)).

Various waste streams have been evaluated for bioH_2 production, such as cheese whey (CW), winery waste, and brewery waste.[12–14] Considering the wastewater organic content and discharge capacity, CW is particularly attractive as a feedstock for bioH_2 production. Out of these different sources of wastewater, the cheese industry consumes a significant amount of water and produces a large amount of wastewater. The U.S. produces around 13 billion pounds of cheese, generating around 3.9 million gallons of CW per day.[15] CW is the waste stream from the cheese industry and has a high organic content.[16] It consists of 93%–94% water, with the rest being lactose, proteins, fats, and other minerals.[17]

Urbanization and population growth have also led to a rapid increase in municipal solid waste, and 22% of it is solid food waste (SFW).[18] In 2018, the U.S. Environmental Protection Agency (EPA) reported a 60% increase in food waste compared to levels in 1990.[19] Food waste is a rich source of carbohydrates and is produced in vast quantities, especially in commercial locations such as restaurants, institutional cafeterias, and residential areas.[20] Thus, CW and SFW are potential feedstocks for bioH_2 production.

Bio-based H_2 production includes thermochemical processes, such as biomass gasification[21–23] and fast pyrolysis,[24,25] as well as biotechnological processes, such as direct and indirect photolysis, photo-fermentation,[26–28] dark fermentation (DF),[29–31] and biomass-driven electrolysis.[32–34] Well-known processes, such as fast pyrolysis, await commercialization owing to the high energy demand during scale up;[35] photofermentation has a major challenge of being light (intensity) dependent, resulting in H_2 yield uncertainty.[36,37]

Dark fermentation (DF) is one of the most widely used techniques for producing H_2 from organic waste residues.[38–41] Compared to photo-based biochemical processes, DF has a higher H_2 concentration yield and fewer requirements for a controlled environment for microorganisms (independent of light intensity).[42,43] Particularly, DF, operated under aqueous conditions, is well suitable for treating aqueous and wet waste streams and generating fresh water.[44] DF is a biochemical conversion of organic matter to bioH_2 that uses microorganisms in the absence of light and oxygen.[45] A techno-economic analysis (TEA) of DF fed by agricultural residues estimated a reduction in H_2 production cost from $50 kg^{-1} (2015 dollars, including byproduct credits) to around $6 kg^{-1} (2025, including byproduct credits) assuming an improvement in technologies with increased studies and experimental work.[46] Hosseinzadeh *et al.*[47] reported that detailed research is required to increase the H_2 productivity from wastewater and biomass to increase commercial viability. Han *et al.* studied the techno-economic analysis of bioH_2 production from waste bread *via* DF, obtaining a final production cost of $15 kg^{-1} H_2.[48] Thus, more investigation is required to scale up plant capacity. From a sustainability viewpoint, DF accounted for greenhouse gas (GHG) emissions of 2.5 kg CO_{2e} kg^{-1} H_2, which is much lower than fossil-based H_2 production.[49] Y. Kannah *et al.*[50] mentioned that dark fermentation-based systems producing H_2 incur comparatively lower production and capital costs than systems employing photo-fermentation.

While DF converts organics (*e.g.*, sugars) to hydrogen, it co-produces fatty acids, such as acetic acid. These fatty acids can be further processed to generate more hydrogen using microbial electrolysis cells (MECs).[51] The following equations show what occurs during dark fermentation and microbial electrolysis, producing bioH_2 from glucose and galactose (DF) and organic acids (MEC).

Dark fermentation:

$$C_6H_{12}O_6(\text{glucose/galactose}) + 2H_2O \rightarrow 2CH_3COOH + 4H_2 + 2CO_2$$

$$C_6H_{12}O_6(\text{glucose/galactose}) \rightarrow CH_3CH_2CH_2CO_2H + 2H_2 + 2CO_2$$

$$C_6H_{12}O_6(\text{glucose/galactose}) + 2H_2O \rightarrow CH_3CH_2CO_2H + 5H_2 + 3CO_2$$

Microbial electrolysis cells:

$$CH_3COOH + H_2O \rightarrow 4H_2 + 2CO_2$$

$$CH_3CH_2CH_2CO_2H + 6H_2O \rightarrow 10H_2 + 4CO_2$$

$$CH_3CH_2CO_2H + 4H_2O \rightarrow 7H_2 + 3CO_2$$

MEC is an emerging technology that removes additional organic matter from wastewater while producing valuable bioproducts, such as H_2.[52] Segundo-Aguilar *et al.*[53] used a double-chambered MEC that uses wastewater from the food industry to produce H_2 at the cathode and biogas at the anode. Breakeven was reached with an H_2 production efficiency of 40%, voltage of 0.3 V, and H_2 and biogas prices of \$5.10 kg^{-1} and \$0.20 m^{-3}, respectively, with a profit of \$0.01 kg^{-1} chemical oxygen demand (COD) removed. This study was performed on a lab-scale basis. Studies have pointed out that MEC is at an early stage of development; thus, a thorough analysis is required, especially during scale-up when performing techno-economic analysis.

MEC systems also have environmental benefits. Chen *et al.*[54] reported a reduction in GHG emissions of around 64% through further process optimization of MEC systems fed by urban wastewater. The study reported GHG emissions of 18.8 kg CO_{2e} kg^{-1} H_2 using the U.S. electricity mix, indicating that carbon intensity can be further reduced using renewable energy resources. The GHG emissions obtained in this study were similar to those of H_2 production *via* coal gasification.[55] Recent studies have indicated that integrating MEC systems with anaerobic digestion,[56] or anaerobic membrane bioreactor,[57] or thermoelectric micro-converter,[58] or microbial fuel cells and dark fermentation[59] could enhance energy generation by recovering various valuable products, providing advantages for their application in the future. Koul *et al.*[60] discussed the significant potential of MEC-integrated systems in forming a future bioeconomy although extensive research is required to increase the product yield and efficiency of the process.

The integration of DF and MEC has been observed to enhance the total bioH_2 yield. Marone *et al.*[61] observed that an integrated DF-MEC system produced 13 times the bioH_2 yield of a standalone DF system. Li *et al.*[62] studied an integrated DF-MEC facility fed by cornstalks and observed around three times the H_2 production of DF alone. An MEC system plays a vital role in additional H_2 production and COD removal from DF effluent, thus making the system environmentally attractive. However, the production cost was not evaluated.

To the best of our knowledge, no studies have evaluated both the production cost and GHG emission reduction potential of bioH_2 produced from an integrated DF-MEC system. This work fills this information gap and evaluates two potential feedstock sources: cheese whey (CW) and solid food waste (SFW).

Methodology

The system analysis in this study is performed in three major steps: (I) process modeling, (II) techno-economic analysis (TEA) and (III) life cycle analysis (LCA).

In the CW-fed scenario, the aqueous feedstock is preheated to 105 °C to remove lactic acid bacteria,[63] cooled, and fed into a fermenter that is maintained at 60 °C. Inoculum is heated to 85 °C and batch-fed into the fermenter (capacity of each fermenter vessel being 1 MM gallon[64]), keeping the CW-to-inoculum volumetric ratio at 2.5 : 1.[14,63] After 48 hours of fermentation, H_2 is generated along with CO_2, and the gas mixture (H_2, CO_2, and water vapor) is directed to a Selexol™ unit, followed by a pressure swing adsorption (PSA) process to separate the CO_2 for sequestration and obtain high purity H_2.[65] In addition, the CO_2 is further purified with a CO_2 capture unit for potential sequestration or sale. The aqueous effluent, which is rich in organic acids (OAs), such as acetic acid, butyric acid, and propionic acid, is fed to the MEC system to produce more H_2 and CO_2. The total CO_2 produced from both processes is collected and compressed to 2200 psi[66] for carbon capture and sequestration (CCS) or to be sold to the beverage industry.

In the SFW feedstock scenario, in addition to the integrated DF-MEC, a pretreatment process, which includes grinding and potassium hydroxide (KOH) treatment, is necessary to size the solid feedstock for conversion efficiency.[67] The net bioH_2 obtained from both scenarios was set at 50 MT day^{-1}, per DOE's targeted production scale.[68]

Process modeling

Using Aspen Plus™ software, we developed two process models to simulate commercial-scale plants with capacities of 50 MT day^{-1} of bioH_2.[69] The CW and SFW feedstock compositions were taken from Moreno *et al.*[14] and Kim and Shin,[67] respectively (Tables S1 and S2†). The dark fermentation operating conditions and yield were set based on previous studies by Davis *et al.*[64,70] and Humbird *et al.*[71] Given the absence of commercial MEC operation, the conceptual commercial scale MEC was designed with the design factors of proton exchange membrane (PEM) and chloralkali electrolyzer systems as studied by Mayyas *et al.*,[72] Escapa *et al.*,[73] and Cusick *et al.*[12] Fig. 1 and 2 show the process flow diagrams of the two 50 MT day^{-1} bioH_2 plants using CW and SFW as feedstock, respectively, with their corresponding stream conditions (denoted by the flow numbers in Fig. 1 and 2) tabulated in the ESI in Tables S2 and S3.† In both bioH_2 plants, the process model undergoes the following sub-processes (also shown in Fig. 1 and 2):

- Handling: Feedstock handling and transportation are reflected in the feedstock cost and life cycle analysis carbon footprint.
- Pretreatment: This applies only to the SFW-fed scenario, where the SFW is ground and treated with KOH to enhance the feedstock-to-H_2 conversion efficiency. The insoluble food waste content (around 40% of SFW, mostly containing bone structure) is separated and disposed of. Owing to incomplete information, we treated the non-soluble solid as lignin. The insoluble solid is not converted or sent for combustion but rather filtered for disposal. In the CW scenario, no pretreatment is required.
- Dark fermentation (DF): In this process, fermentation occurs in the absence of O_2 to generate H_2, CO_2, organic acids, and other by-products, such as ethanol.[29] In the SFW scenario, the SFW loading to the fermenter is assumed to be 50 g L^{-1}.[74]

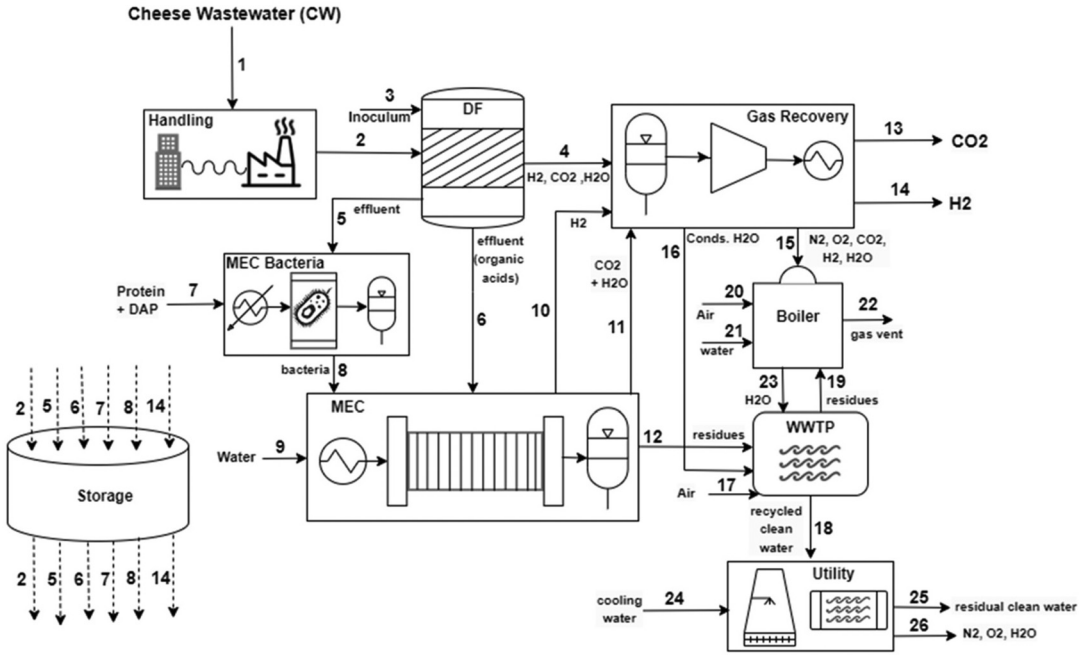

Fig. 1 Detailed process flow diagram showing 50 MT day^{-1} bioH_2 production from CW through DF-MEC integration.

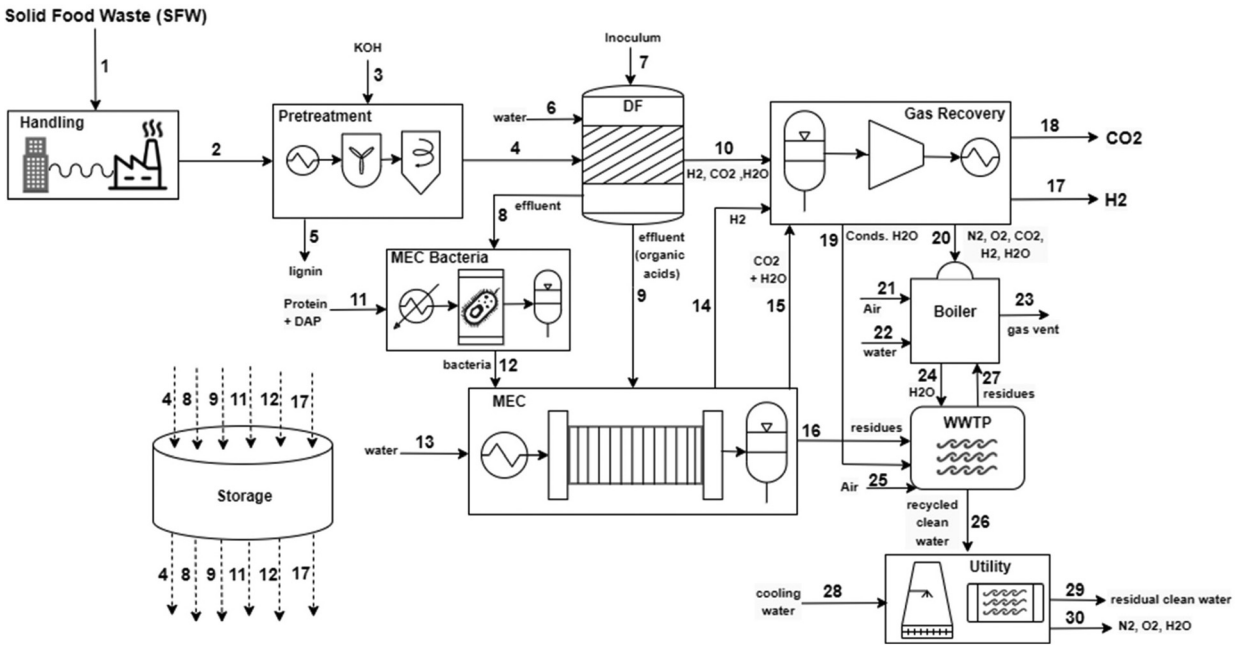

Fig. 2 Detailed process flow diagram showing 50 MT day^{-1} bioH_2 production from SFW through DF-MEC integration.

The gaseous product from DF contains H_2, CO_2, and H_2O, which go to the gas recovery section for separation using the Selexol unit and pressure swing adsorption (PSA). For both scenarios, we assumed that DF occurs at 60 °C and 1 bar for 48 hours, reaching a conversion rate (of sugars) of approximately 80%, using validated test results.[75] From previous literature studies of waste materials to bioH_2 production through DF, it is observed that acetic acid formation is highest, followed by butyric and propionic acid.[13,61,65,74–85] Hence, based on prior literature reviews, we assumed that 51% of glucose produces acetic acid (along with H_2 and CO_2), while 24% and 5% of glucose produce H_2 and CO_2 through the production of BA and PA, respectively, which are further reutilized during MEC.

• MEC bacteria: This step involves bacteria production using effluents from DF along with protein and diammonium phosphate (DAP) (nutrients required for bacterial growth) based on a process developed in previous studies.[86] For both CW and SFW scenarios, we assumed that the MEC conversion of organic acid is 90%.[87]

• Microbial electrolysis cell (MEC): In this process, the DF effluent, containing acetic acid, butyric acid, and propionic acid (CW scenario only), is utilized by microorganisms at the anode side to generate electrons and protons at a very low voltage. The electrons go to the cathode side and reduce protons to produce H_2.[60] The MEC effluent, with other remaining organics and impurities, is fed to the WWTP. For both scenarios, organic acid loading is set at 10 g L^{-1}.[88]

• Gas recovery: This section separates the H_2 and CO_2 gas streams from the DF gaseous product. The effluent goes through a glycol process, commercially called Selexol,[65] for the recovery of CO_2, followed by a pressure swing adsorption (PSA) process[89] that separates CO_2 and H_2 gases. The PSA process is modeled using a reference design adopted from Spath *et al.*[89] report, assuming an 85% H_2 recovery rate. MEC generates high-purity H_2 and CO_2 from the cathode and anode, respectively; thus, only compression is needed. The byproduct CO_2 is compressed to 2200 psi (or 150 atm) for further storage and transportation[66] and thus can be either sold to the beverage industry or sent to geological sequestration sites.

• Boiler: This process involves the generation of steam and onsite electricity *via* the combustion of unused components of DF and MEC.

• Wastewater treatment plant: This step includes the treatment of wastewater before it is discharged to the environment, and a portion of the treated water is recirculated and used to meet process water requirements. No additional process water is required since both feedstocks are around 88% water.

• Utility: This section consists of a cooling tower and recycling of the treated water from the WWTP to meet process requirements.

• Storage: This section primarily involves the storage of process chemicals.

The purity of product H_2 for both feedstock scenarios is 99.99% with 290 psi (or 20 atm), while that of CO_2 is 99.8% with 2200 psi (or 150 atm). For the dark fermentation bacteria production, we assumed a bacteria loading of 3.5×10^{-4} g g^{-1} sugars based on a previous study of bioH_2 production from corn stover[46] since there is no such information available about using CW and SFW as feedstocks.

Life cycle analysis

LCA is widely used to quantify the environmental impacts and carbon footprint of a product. The LCA evaluation used in this study follows the International Organization for Standards (ISO) 14040 and 14044.[90,91] The Greenhouse Gases, Regulated Emissions, and Energy Use in Technologies (GREET)[92] 2022 model was employed to quantify the life cycle GHG emissions of bioH_2 produced from two conceptual plants using CW and SFW as feedstocks. This is a well-to-gate analysis that includes all stages along the bioH_2 supply chain, starting from energy recovery and raw material extraction to the bioH_2 product delivered at the plant gate ready for transportation to downstream customers. Table 1 lists the carbon intensities of all resources consumed in the conceptual bioH_2 plants modeled in this study. For both cases, we assumed that the waste streams are burden free and that the two plants are located at the site where the waste is accumulated. Both scenarios were normalized to a functional unit of 1 kg H_2 for comparison purposes. The power required by both plants is assumed to be sourced either from the U.S. electricity grid mix or from renewable resources.

Table 1 GHG emission factors of resources required for bioH_2 production from CW- and SFW-fed plants[6]

Resources	Emission factor (kg CO_{2e} kg^{-1} or kW h)
U.S. electricity grid mix	0.44
Corn steep liquor	1.72
Diammonium phosphate	1.74
KOH	1.80
Nutrients in the CW scenario	0.52
Nutrients in the SFW scenario	1.64

After obtaining the LCA results, H_2 production cost graphs in the TEA section for both feedstock scenarios were compared based on the 2022 U.S. Inflation Reduction Act's 45 V credits for H_2 production[93] and 45 Q credits for carbon capture and sequestration.[94] These potential tax credits enable the facilities to earn additional production tax credits (PTCs) depending on the life cycle GHG emissions from the H_2 plant and CO_2 captured and sequestered, and they last for 10 years in the 45 V case and 12 years in the 45 Q case. Only one of the potential PTCs is accounted for at a time. Related information is provided in Table S7† and shown in the TEA result section.

We further quantified the water consumption factor (WCF) for the two plants using the following equation:

$$\mathrm{WCF} = -\frac{W_\mathrm{p}\left(\mathrm{gal\,h^{-1}}\right) - W_\mathrm{pr}\left(\mathrm{gal\,h^{-1}}\right) - W_\mathrm{e}\left(\mathrm{gal\,h^{-1}}\right)}{H_2\ \mathrm{rate}\left(\mathrm{kg\,h^{-1}}\right)}$$

where W_p is the clean water produced by the WWTP section, W_pr is the water recycled to be used by the integrated DF-MEC system, and W_e is the water consumption rate for electricity usage. The water consumption rates for electricity (U.S. mix, wind, and solar) are 0.59 gal kW^{-1} h^{-1}, 0.001 gal kW^{-1} h^{-1} and 0.12 gal kW^{-1} h^{-1}, respectively.[6] There is a minus (negative) sign at the beginning of the equation since both plants produce clean water on a net basis.

Techno-economic analysis (TEA)

The economic feasibility of the two plants was evaluated using the U.S. Department of Energy (DOE) supported hydrogen analysis (H2A) production models[68] to obtain the levelized bioH_2 production cost. The bioH_2 production cost was estimated with a discounted cash flow rate of return analysis using a 10% internal rate of return (IRR) over the project lifetime of 40

years operating at 90% capacity. For this purpose, annual expenditure, revenues, and investment costs were estimated. Annual expenses (or operating costs) primarily included fixed costs (*e.g.*, labor and maintenance costs), raw materials, and energy expenses. Revenues earned depended on how the plants chose to utilize the byproduct CO_2. Finally, the investment (or capital costs) primarily consisted of the purchase and installation costs of all the equipment, working capital, depreciation over the period, indirect project construction costs, *etc*. All cost estimates are based on 2019 U.S. dollars. Table 2 shows the economic assumptions for the two $bioH_2$ plants. Table 3 shows the material and energy flows and costs for the two plants. An Aspen Process Economic Analyzer[95] was used to size the equipment across all operating units of the two Aspen Plus models and estimate the equipment costs of the two plants. In the case of the MEC system, we assumed current densities of 20 A m^{-2}, 50 A m^{-2} and 100 A m^{-2} based on experimental results by Jeremiasse *et al.*,[96] Miller[97] and Liu *et al.*,[98] respectively. These MEC studies used wastewater and biomass as feedstock, using graphite/graphite felt as the anode and Ni foam/MoP as the cathode. From reported MEC test results using various feedstocks at different scales, the current density varies greatly from approximately 2.5 A m^{-2} (ref. 73) up to 100 A m^{-2},[97,98] as summarized in Table S4.† Based on the available literature data, the median MEC current density value is around 20 A m^{-2}. Thus, this study shows TEA results based on three MEC operating current densities and evaluates their impact on the economics of the two plants (since with an increase in current density, the material required for MEC decreases and *vice versa*). The median of current density (20 A m^{-2} (ref. 96)) is used to estimate the $bioH_2$ production costs based on current MEC operations. The higher and more optimistic MEC current densities of 50 A m^{-2} and 100 A m^{-2} are used to evaluate their impact on the $bioH_2$ production cost.[97,98] The MEC stack design was adopted from the literature based on commercially available proton exchange membrane (PEM) water electrolyzers and chloralkali electrolyzers.[12,72,73] Some of the key assumptions in the MEC design, *e.g.*, cost information, are provided in Tables S5 and S6 of the ESI.† We note that MEC operating at 20 A m^{-2} has graphite felt and Ni foam as electrode materials[96] while MEC operating at 50 A m^{-2} and 100 A m^{-2} has graphite and MoP as electrode materials,[97,98] as shown in Table S6.† In Table S5,† the study assumed MEC active areas of 2 m^2 and 0.3 m^2. The latter value (0.3 m^2) is taken based on NREL's 2021 technical report on PEM electrolyzers,[99] which is ongoing. The 2 m^2 value is taken from Brinkmann *et al.*'s study of industrial-scale chlor-alkali plants.[100] Our study primarily focuses on the results derived from Brinkmann *et al.*[100] since that study is based on common industrial practices. The $bioH_2$ production costs, based on a 0.3 m^2 active area of the MEC electrode,[99] are included in the ESI in Fig. S1 and S2.†

Our study points out that since both feedstocks are (bio-based) waste streams, both have the advantage of earning additional revenues through discharge or landfill tipping (disposal) fees charged to the waste producers. For SFW, the tipping fee is assumed to be around \$53 MT^{-1} of solid waste disposed of,[116] which is a typical municipal solid waste disposal fee in the U.S. For this study, we considered a net tipping fee of \$32 MT^{-1} of solid waste since we are disposing of 40% of the insoluble SFW as lignin, as mentioned above. In the case of CW, the discharge fees heavily depend on the COD, total suspended solid (TSS) contents in the wastewater, and the location of the plant. The four governing equations[117] used to calculate the net discharge fees are as follows:

$$D_f = S_t + D_h + V_f, \quad (1)$$

Table 2 Financial assumptions for the two 50 MT day^{-1} $bioH_2$ plants[68,72]

Parameters	Assumptions
Plant life	40 years
After tax IRR	10%
Construction period	3 years
Start-up time	1 year
Income tax rate	25.74%
Salvage value	10% of depreciable capital investment
Revenue and costs during start-up	Fixed costs: 100% Variable costs 75% Revenue: 50%
Equity	40%
Interest rate on debt financing	3.7%
Working capital	15% of the yearly difference in operating costs
Salvage value	10% total capital investment
Decommissioning costs	10% of depreciable capital investment
Depreciation schedule	20 years, MACRS

Table 3 Material and energy flows and costs/revenue (2019 USD) for CW and SFW plants producing 50 MT day^{-1} $bioH_2$

Materials/energy input	Flowrate (MT or MW h day^{-1})	Price	Ref.
CSL	0.03 (CW), 0.04(SFW)	\$0.036 lb^{-1}	71
DAP	0.02 (CW), 0.003(SFW)	\$0.63 lb^{-1}	71
KOH	0 (CW), 72 (SFW)	\$0.71 kg^{-1}	101
Nutrients in the CW scenario	194.6	\$4.30 kg^{-1}	102–113
Nutrients in the SFW scenario	0.1	\$1.10 kg^{-1}	110
Industrial electricity	916.7 (CW), 1089 (SFW)	\$0.067 kW^{-1} h^{-1}	114
CO_2[a] (used in beverage industry)	490.2 (CW), 492.7 (SFW)	\$0.10 kg^{-1}	115

[a] Not the cost but revenue earned through CO_2 sales in the beverage industry.

where D_f = net discharge fees, S_t = strength charge, D_h = domestic holding tank fees or rate, and V_f = volume discharge fees (also referred to as the industrial capacity discharge rate).

$$S_t = [V \times (\mathrm{TSS} - 250) \times 8.34 \times \mathrm{TSS}_{rate}] + [V \times (\mathrm{COD} - 500) \times 8.34 \times \mathrm{COD}_{rate}] \quad (2)$$

where V = the volume of the waste stream in million gallons per year (MGPY); TSS = amount of suspended solid in mg L^{-1}; COD = amount of chemical oxygen demand in mg L^{-1}; 8.34 = designated conversion rate; TSS_{rate} = \$ lb^{-1} of excess TSS present, depending on the region; and COD_{rate} = \$ lb^{-1} of excess COD present, which again depends on the region.

$$D_h = \frac{\$P}{1000\,\text{gallons}}, \quad (3)$$

where P = the designated amount for the holding tank, which usually remains the same throughout.

$$V_f = \frac{\$Q}{1000\,\text{gallons}}, \quad (4)$$

where Q = the designated amount for discharging the liquid waste streams.

The TSS, COD, domestic tank, and industrial wastewater discharge fee rates assumed for each region are shown in Table 4. Using eqn (1)–(4), Table 5 shows that the revenue earned through the discharge fee is highest for the western U.S. region (California), followed by those of the southern and midwestern U.S. regions.

Table 4 TSS, COD, domestic tank and industrial wastewater discharge fee rates considered for each region

Regions in the U.S.	TSS_{rate} (\$ lb^{-1})	COD_{rate} (\$ lb^{-1})	P	Q	Ref.
Midwest	0.413	0.21	11.4	3.1	117
South	0.27	0.26			118
West	1.14	0.43			119

Table 5 Revenue earned through discharge and tipping fees of CW and SFW feedstocks, respectively, by the 50 MT day^{-1} $bioH_2$ plant

Regions in the U.S.	Cheese whey wastewater discharge fees \$ kg^{-1} CW (or \$ kg^{-1} H_2)	Solid food waste (net) tipping fees \$ kg^{-1} SFW (or \$ kg^{-1} H_2)
Midwest	−0.057 (−5.6)	−0.032 (−2.9)
South	−0.064 (−6.3)	
West	−0.11 (−11.3)	

Results and discussion

Life cycle analysis (LCA)

Fig. 3 and 4 illustrate the life cycle GHG emissions of $bioH_2$ produced from the two plants. Various scenarios assuming different sources of electricity supply and CO_2 byproduct utilization methods were assessed, and the scenarios were compared based on these factors. The scenarios were also compared to existing facilities producing H_2 from natural gas (NG) *via* SMR with and without carbon capture and sequestration (CCS) facilities and *via* proton exchange membrane (PEM) water electrolysis systems using U.S. mix, wind, and solar electrical energy inputs. These are designated by the dashed-dot,

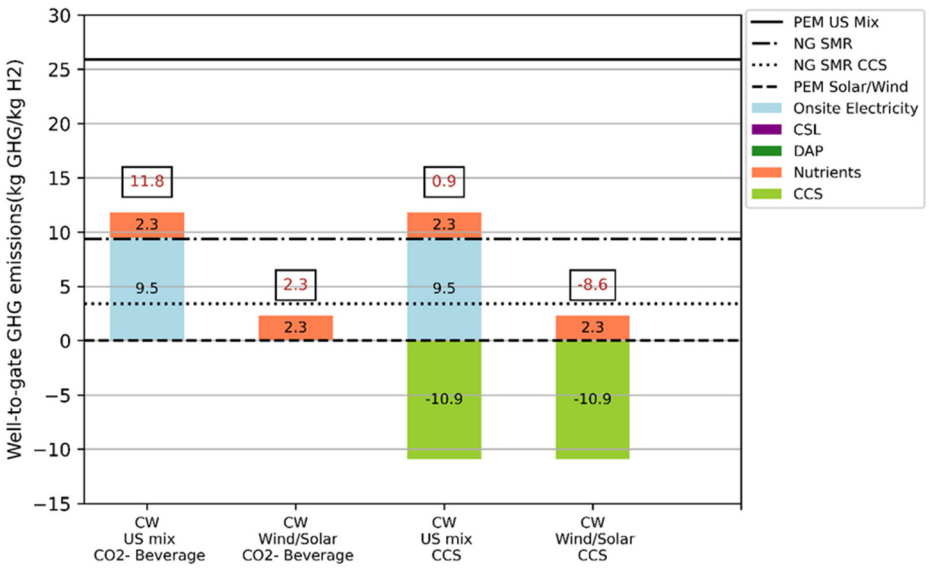

Fig. 3 Well-to-gate GHG emission comparison of different electricity sources and byproduct CO_2 utilization for a 50 MT day^{-1} plant producing H_2 from CW through DF-MEC integration.

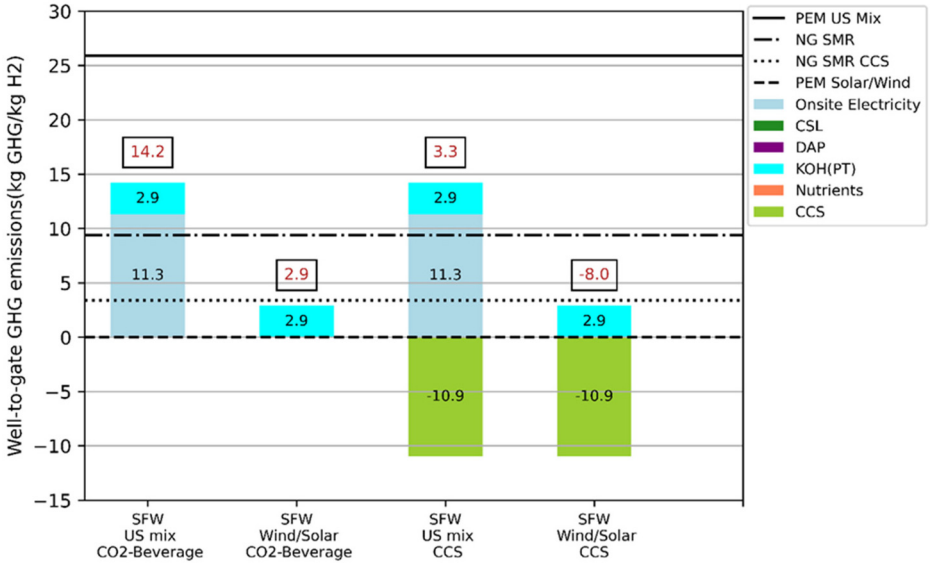

Fig. 4 Well-to-gate GHG emission comparison of different electricity sources and byproduct CO_2 utilization for a 50 MT day^{-1} plant producing H_2 from SFW through DF-MEC integration.

dotted, dashed, and solid lines, respectively, illustrated in Fig. 3 and 4.

In both scenarios, when the U.S. mix electricity is used, electricity is the main source of GHG emissions, accounting for 9.5 kg GHG kg^{-1} H_2 in the CW scenario and 11.3 kg GHG kg^{-1} H_2 in the SFW scenario. Electricity GHG emissions are zero when the source is renewable. In the SFW scenario, the GHG emissions from the U.S. mix electricity are around 18% higher than in the CW scenario owing to the additional pretreatment required. This shows that the life cycle GHG emissions for both scenarios are sensitive to the electricity input rate and source.

The use of nutrients (trace elements required by bacterial growth) in the CW scenario contributes 2.3 kg GHG to the life cycle GHG emissions of bioH_2, while their impacts in the SFW scenario are negligible. This is because the CW scenario requires more nutrients than the SFW scenario. The SFW scenario, however, incurs a GHG emission of 2.9 kg GHG kg^{-1} H_2 from the KOH required for pretreating the SFW, which is not required in the CW scenario.

For both scenarios, using the CCS technology to capture and sequester byproduct CO_2 constitutes a major GHG sink, which further helps in achieving negative life cycle GHG emissions for both scenarios when the electricity source is renewable. This, in turn, reduces the net H_2 production cost through a PTC of \$3 kg^{-1} H_2 (Table S7†) for both plants. PTCs of \$0.75 and \$1.00 kg^{-1} H_2 are assumed for the second and third cases of the CW scenarios, respectively. For the SFW scenarios, the PTC assumed for both the second and third cases is \$0.60 kg^{-1} H_2.

Water consumption factor

This study also quantified the water consumption factor (WCF) since two plants (Table 6) require process water. Table 6 shows the water consumption factors of the two plants using different electricity sources. The WCFs are all negative since both plants use the organic content of the wastewater to produce bioH_2 and clean water. A portion of this clean water is used by the integrated DF-MEC process and electricity generation, and the rest can be discharged into the environment. All scenarios discharge clean water to the environment, unlike conventional H_2 production pathways, such as SMR and PEM electrolysis, which have WCFs of 2.4 and 4.1 gal kg^{-1} H_2, respectively.[120] Thus, none of them incur the cost of buying process water.

Table 6 Water consumption factors of CW- and SFW-fed plants producing 50 MT H_2 day^{-1} with different electricity resources

Scenario	Net water discharged (MM gal h^{-1})	WCF (gal kg^{-1} H_2)
CW—U.S. mix	0.03	−16
CW—wind	0.05	−28
CW—solar	0.048	−26
SFW—U.S. mix	0.02	−13
SFW—wind	0.05	−27
SFW—solar	0.045	−24

Techno-economic analysis (TEA)

Fig. 5(a)–(e) show the installed equipment costs required by the two plants and MEC operating at 20 A m^{-2}, 50 A m^{-2} and 100 A m^{-2} current density, each producing 50 MT day^{-1} of bioH_2. To produce 50 MT day^{-1} bioH_2, the installed equipment costs at 20 A m^{-2}, 50 A m^{-2} and 100 A m^{-2} for the CW plant are \$3398 million (MM), \$1265 million MM and \$711 MM, respectively. The same for SFW plants are \$3918 MM, \$1465 MM and \$832 MM at 20 A m^{-2}, 50 A m^{-2} and 100 A m^{-2}, respectively. The total project investments for the 50 MT day^{-1} bioH_2 plant are \$4826 MM, \$1798 MM and \$1010 MM for a

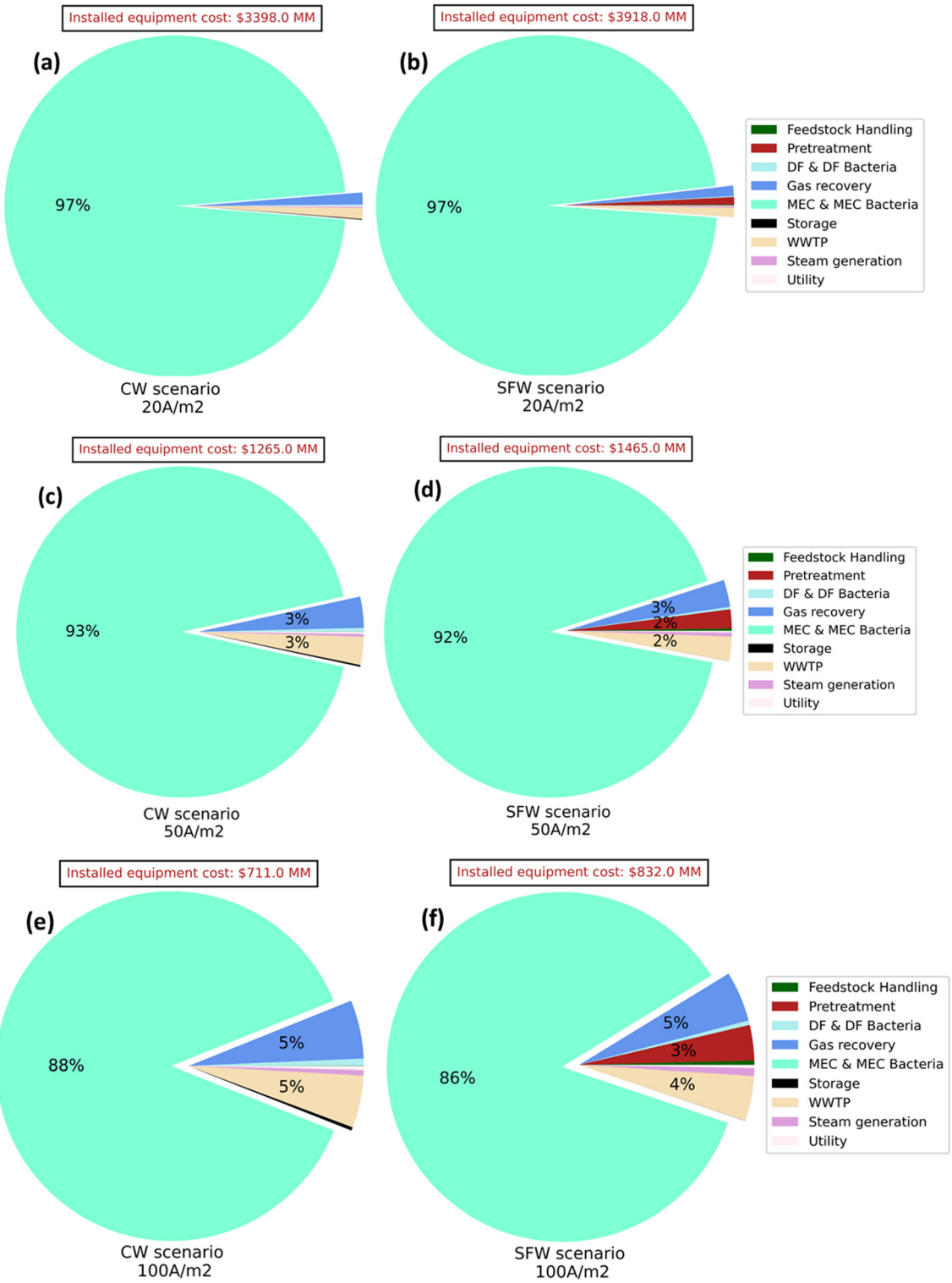

Fig. 5 Installed equipment costs for (a) CW to 50 MT day^{-1} bioH_2, (b) SFW to 50 MT day^{-1} bioH_2 MEC operating at 20 A m^{-2}, (c) CW to 50 MT day^{-1} bioH_2, (d) SFW to 50 MT day^{-1} bioH_2 with the MEC operating at 50 A m^{-2}, (e) CW to 50 MT day^{-1} bioH_2 and (f) SFW to 50 MT day^{-1} bioH_2 with the MEC operating at 100 A m^{-2} *via* the DF-MEC integration pathway.

CW-fed plant and $5564 MM, $2081 MM and $1181 MM for an SFW-fed plant with an MEC section operating at current densities of 20 A m^{-2}, 50 A m^{-2} and 100 A m^{-2}, respectively. The total project investment includes total direct capital costs, engineering costs, site preparation, project contingency, licensing, permits, and land costs. The SFW plant incurs additional

costs of around 1%–3% for feedstock pretreatment with KOH and separation of insoluble SFW content. No pretreatment is required for CW plants.

For both plants, the MEC system is the main contributor to the installed capital costs, averaging approximately 92% of the total installed equipment cost for the three MEC operating current densities. Considering both the CW and SFW-fed plants, for the 20 A m^{-2} scenario, 97% of the installed capital costs are incurred by the MEC system, followed by 92% for 50 A m^{-2} and around 85% for 100 A m^{-2}. This is also because the anode (graphite felt – \$290 m^{-2}) used for the 20 A m^{-2} scenario[96] is more expensive than the anode (graphite plate – \$20 m^{-2}) used for 50 A m^{-2} and 100 A m^{-2},[97,98] as shown in Table S6.† Thus, increasing the current density 5 times (20 A m^{-2} to 100 A m^{-2}) reduces the installed capital cost by approximately 78% for both CW and SFW scenarios. This suggests the imperative need to increase the MEC current density as well as to use less expensive electrode materials to reduce the capital costs of the overall plants. Tables S5 and S6† present the stack design parameters, the materials, and the costs of the primary MEC stack design materials. The detailed breakdown of MEC assembly costs for both plants at 20 A m^{-2}, 50 A m^{-2} and 100 A m^{-2} MEC current densities is shown in Fig. 6. At approximately 30% and 24%, the membrane and transportation layer are the two largest contributors to the final MEC assembly cost, respectively, for both CW and SFW scenarios. From Fig. 6, it is observed that for both scenarios, increasing the current density from 20 A m^{-2} to 100 A m^{-2} decreases the total MEC cost assembly by approximately 80%. This further decreases the total installed capital cost by around 78% for both scenarios, as shown in Fig. 5 (comparing a and b *versus* e and f).

In both scenarios, the MEC section needs to operate at a much higher current density to decrease total capital costs. At present, the MEC current densities considered for this study are 20 A m^{-2}, 50 A m^{-2} and 100 A m^{-2},[97,98] which is much lower than a PEM electrolyzer operating at a current density of approximately 17 000–30 000 A m^{-2}.[72,121] Further research is required to increase the operating current density of MEC to aid in reducing the total capital cost and thus the final H_2 production costs.

The 50 MT day^{-1} bioH_2 production cost contributors for the CW and SFW plants, operating at MEC current densities of 20 A m^{-2}, 50 A m^{-2} and 100 A m^{-2} are shown in Fig. 7 and 9, respectively. The CW scenarios have lower bioH_2 production costs at 50 and 100 A m^{-2}, ranging from \$7.2 (at 50 A m^{-2}) and \$2.9 (at 100 A m^{-2}) in the U.S. Midwest region to \$1.5 (at 50 A m^{-2}) and −\$2.8 (at 100 A m^{-2}) in the U.S. west region per kg H_2 produced, assuming the U.S. grid mix as the electricity resource and by-product CO_2 being sold to the beverage industry. The production costs are comparatively higher for the SFW scenario, ranging from \$11.0 (at 50 A m^{-2}) to \$6.1 (at 100 A m^{-2}) per kg H_2, assuming the U.S. grid mix as the electricity resource and by-product CO_2 being sold to the beverage industry.

Another point of comparison for both feedstock scenarios, reflected in the H_2 production cost graphs of the second, third, fourth and fifth scenarios in Fig. 7 and 9, is additional tax credits obtained through the 2022 IRA 45 V and 45 Q credits for H_2 production[93] and carbon sequestration,[94] respectively. Each TEA plot for both scenarios is compared based on electricity input and CO_2 usage. The electricity cost (\$ kW^{-1} h^{-1}) remains the same for all scenarios considered, both U.S. mix and wind/solar power; the difference lies in the life cycle GHG emissions shown in Fig. 3 and 4. The LCA results with different electricity input and CO_2 usage govern the amount of tax credits obtained through the 2022 IRA 45 V, as shown in Table S7,† and thus affect the net bioH_2 production costs. One noticeable thing for both plants (CW and

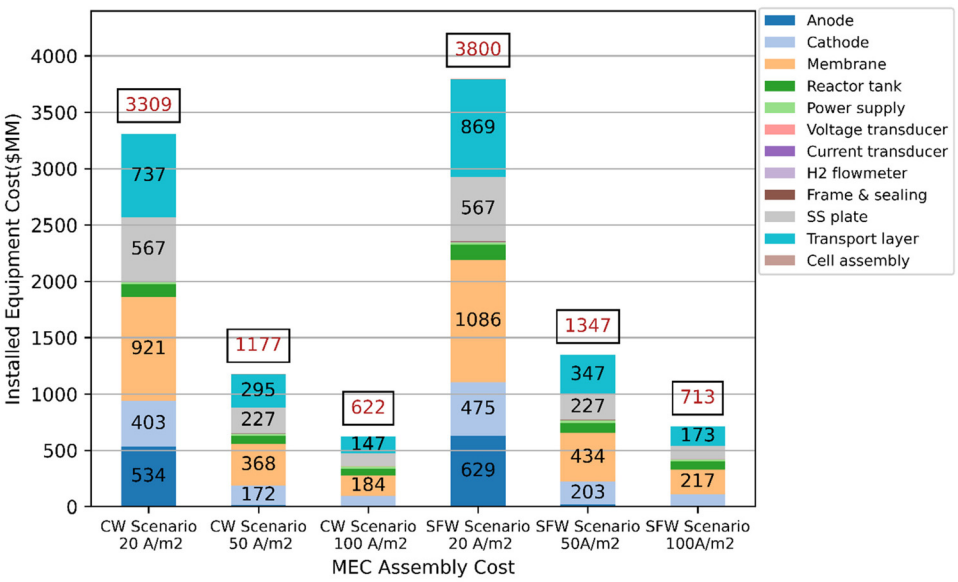

Fig. 6 Installed equipment costs of the MEC assembly for CW and SFW scenarios.

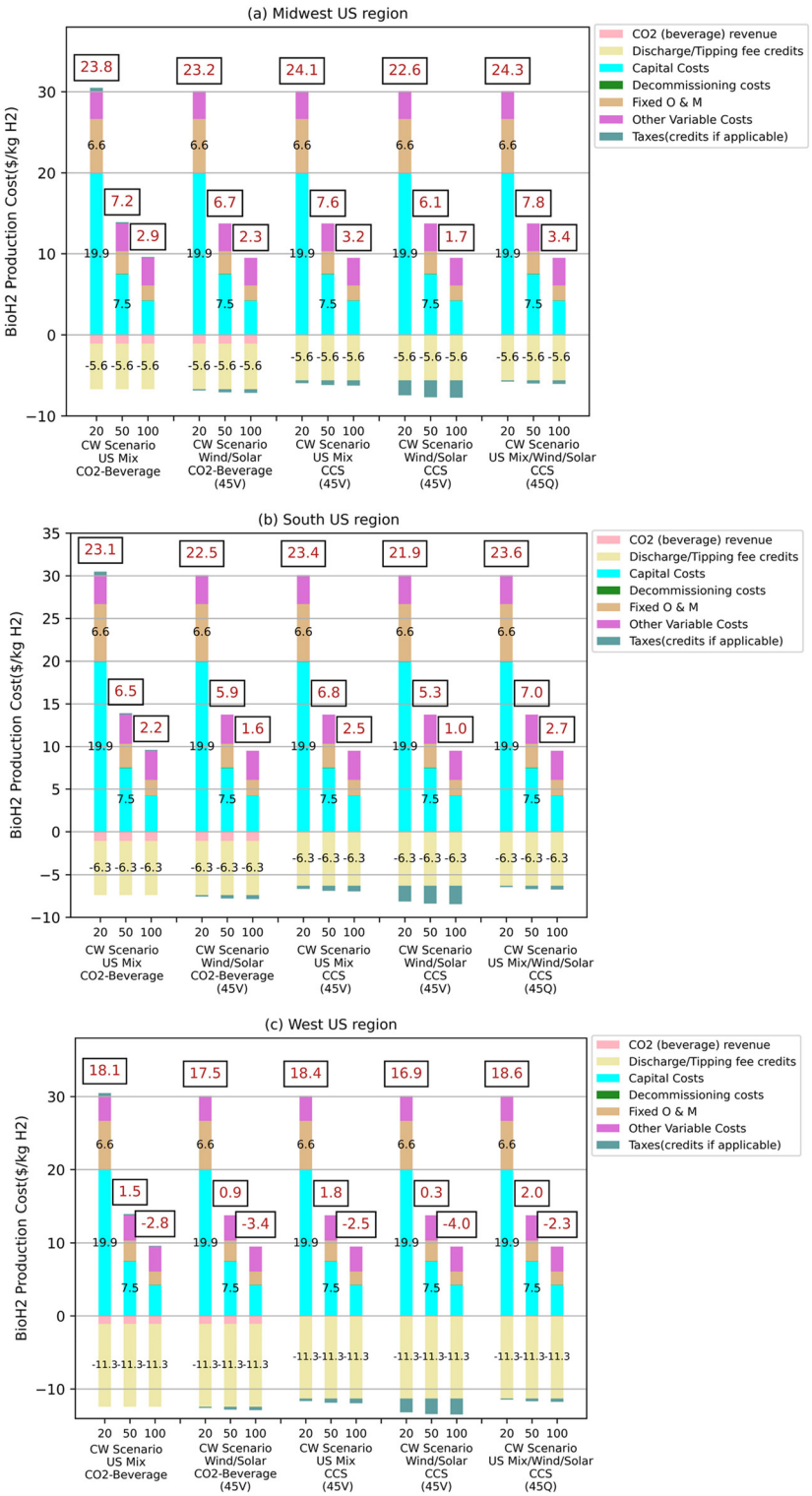

Fig. 7 Contributions to the levelized bioH_2 production cost of an integrated DF-MEC facility producing 50 MT day^{-1} H_2 from CW based on the plant located in (a) the midwestern U.S., (b) south U.S., and (c) west U.S. regions, with the current density of MEC being 20 A m^{-2}, 50 A m^{-2} and 100 A m^{-2}, given the source of electricity supply, byproduct utilization, and potential tax credits earned (if applicable) for each case.

SFW) is that, with an MEC current density of 20 A m^{-2}, the facilities are not economically viable. The lowest bioH_2 production cost achieved is \$16.9 kg^{-1} H_2 for the western US region- CW scenario and \$29 kg^{-1} H_2 for the SFW scenario (assuming renewable energy as an electricity resource with CCS technology and IRA 45 V tax credits).

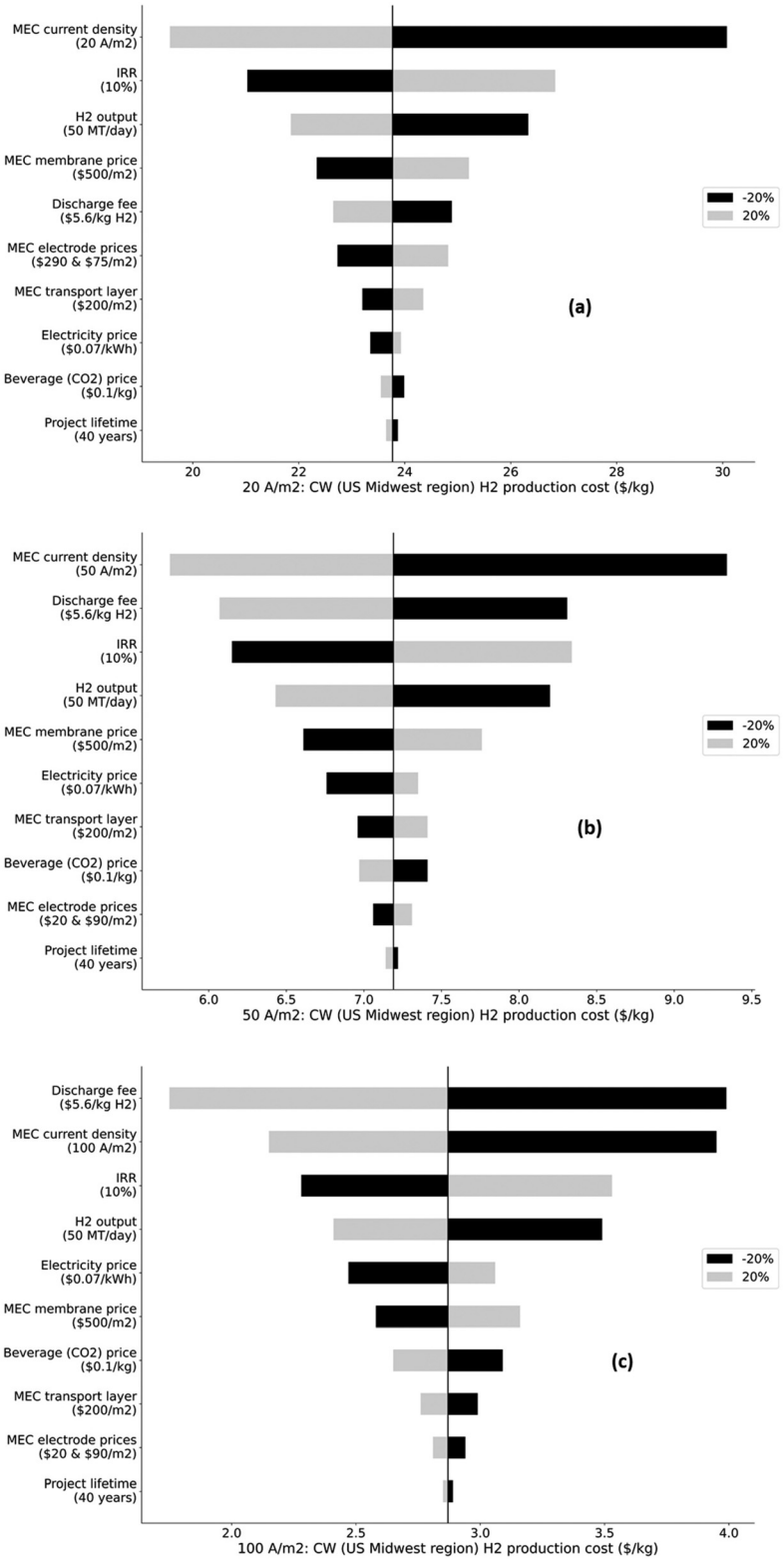

Fig. 8 Sensitivity analysis of H_2 production cost from CW *via* DF-MEC integration producing 50 MT day^{-1} of H_2 based on plants located in the Midwest U.S. region with MEC operating at (a) 20 A m^{-2}, (b) 50 A m^{-2} and (c) 100 A m^{-2}. The labels include the baseline values of each parameter considered.

Fig. 7(a)–(c) show the contributions of different parameters towards the production cost of 50 MT day^{-1} bioH_2 across the U.S. midwestern, southern, and western regions, respectively. Each scenario and location are also compared based on MEC operating conditions of 20 A m^{-2}, 50 A m^{-2} and 100 A m^{-2} current densities to understand the importance of increasing the MEC current density for bioH_2 production.

When CW is used as the feedstock, discharge fee revenues play the largest role in reducing the production cost of H_2, followed by the utilization of the CO_2 by-product, which in turn affects the corresponding PTC obtained by the facility. The discharge fees, as mentioned above, depend on the plant location. High discharge fees in the western region of the U.S. ($11.3 kg^{-1} H_2) lead to negative H_2 production costs (Fig. 7c at 100 A m^{-2}) owing to the increased revenues earned. Other than capital costs, electricity and required nutrients are the main contributors to a variable cost of around $3.30 kg^{-1} H_2 for all three regions shown in Fig. 7.

Fig. 8a–c show the sensitivity of the levelized H_2 production cost from CW to different process parameters. The baseline scenario uses the U.S. mix as the electricity source and assumes selling CO_2 to the beverage industry. We varied each parameter, one at a time, by ±20% and explored the effects on the H_2 production cost. For Fig. 8b and c (MEC current densities being 50 and 100 A m^{-2}, respectively), the H_2 production cost is mostly sensitive to variations in four parameters, with the most influential one being MEC current density, followed by discharge fees, IRR, and H_2 output. Increasing the MEC current density or discharge fees by 20% decreases the H_2 production cost by around 30% and 16% at 50 A m^{-2}, respectively. At 100 A m^{-2}, the discharge fee is more sensitive than the MEC current density. Increasing the discharge fee by 20% decreases the H_2 production cost by 38%, while the same for the MEC current density (baseline being 100 A m^{-2}) is around 30%. In regions where the discharge fee is higher, such as the western U.S., the variations in discharge fees become the most influential factor, surpassing the MEC current density (Fig. S3 and S4†). An increase in the MEC current density decreases the MEC area (or the corresponding MEC stack materials required), which significantly decreases the final bioH_2 production cost. The impact of the final bioH_2 cost due to the discharge fee heavily depends on the region considered, as discussed in Tables 4 and 5.

Similar to the MEC current density and discharge fee, the H_2 production amount shows a similar indirect proportionality relationship (an increase in the parameter decreases the levelized bioH_2 production cost) with the overall production cost. However, increasing the required IRR by 20% increases the H_2 production cost range by approximately 15–20% for the midwestern U.S. region (operating at 50 and 100 A m^{-2} MEC current densities), showing a directly proportional relationship of IRR with the production cost of H_2. Similar patterns are also observed for MEC membrane, MEC transport layer and electrode (cathode and anode) costs. Sensitivity analyses for the southern and western U.S. regions are shown in Fig. S3 and S4.† Fig. 8a shows the sensitivity of the 20 A m^{-2} MEC current density on the bioH_2 production cost. The most sensitive parameter is the current density, which is similar to that observed for the 50 A m^{-2} case (Fig. 8b). Unlike 50 A m^{-2} and 100 A m^{-2}, for MEC operation at 20 A m^{-2}, the discharge fee plays a much less significant role, which is also observed for the south and west U.S. regions for the CW scenario (Fig. S3a and S4a†). This furthermore supports the need for increased MEC current density operation so that the revenues earned through CW (feedstock) at different locations can gain potential signifi-

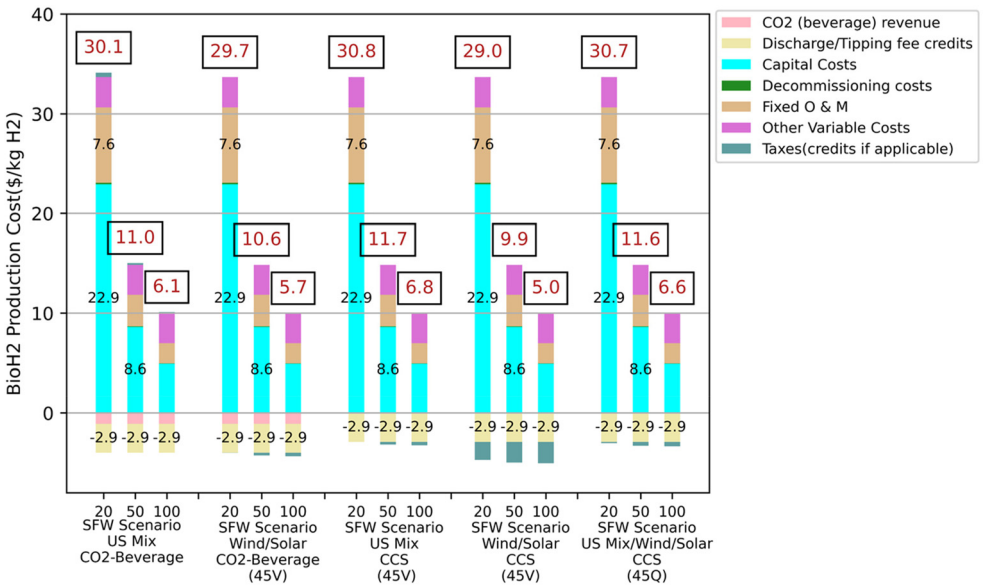

Fig. 9 Production cost breakdown for an integrated DF-MEC facility producing 50 MT day^{-1} H_2 from SFW, with MEC operating current density being 20 A m^{-2}, 50 A m^{-2} and 100 A m^{-2}, based on source of electricity supply, byproduct utilization, and PTC earned (if applicable) for each case.

cance, especially for the west U.S. region. Another point of difference observed in Fig. 8a–c is that for the 20 A m^{-2} case, the MEC electrode prices are much more sensitive parameters for the bioH_2 production cost compared to 50 A m^{-2} and 100 A m^{-2} cases, which is also observed for the SFW bioH_2 production cost sensitivity analysis in Fig. 10. This suggests the

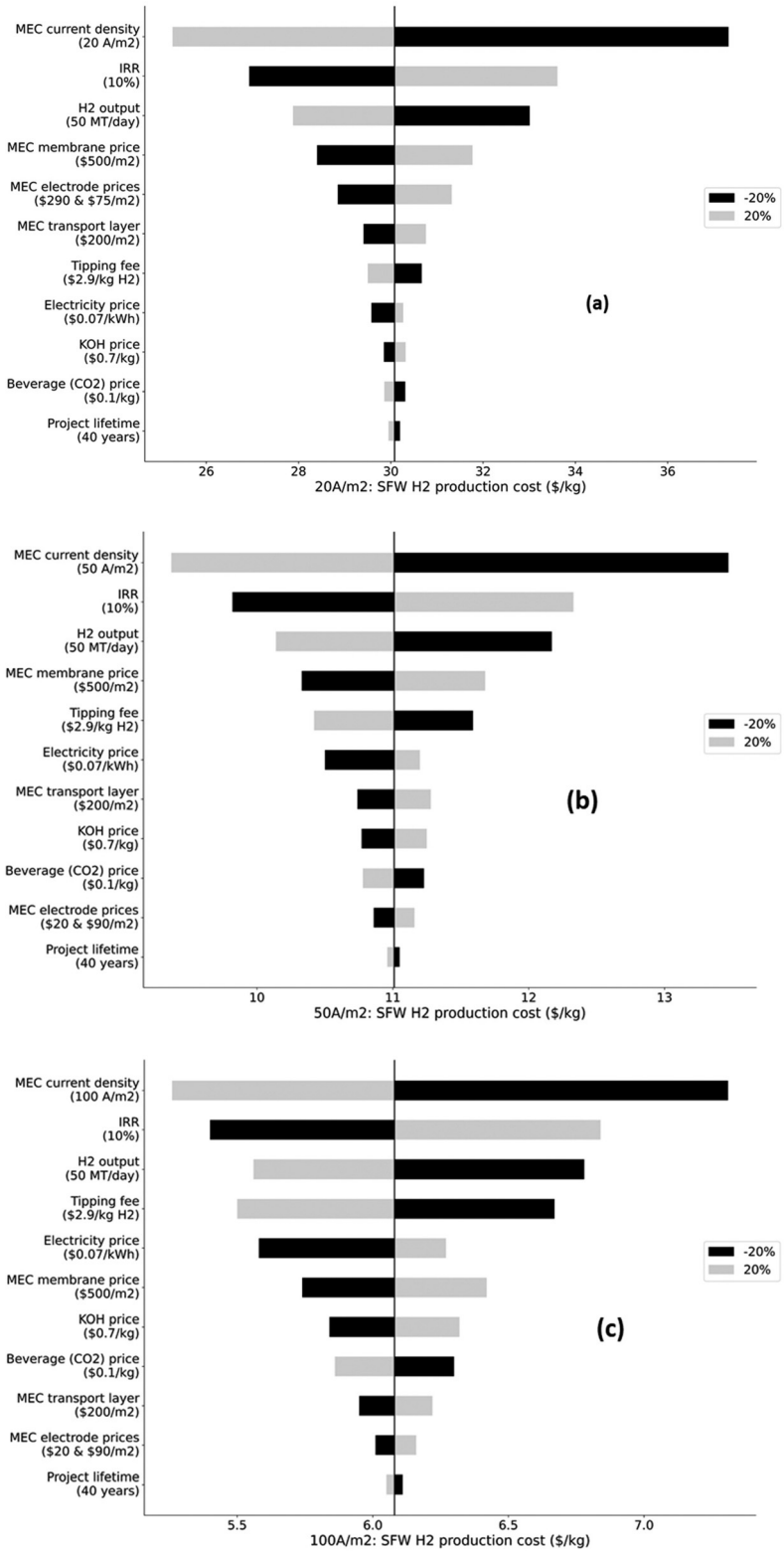

Fig. 10 Sensitivity analysis of H_2 production cost from SFW *via* DF-MEC integration producing 50 MT day^{-1} of H_2, with MEC current density operation being at (a) 20 A m^{-2}, (b) 50 A m^{-2} and (c) 100 A m^{-2}. The labels include the baseline values of each parameter considered.

need for cheaper MEC electrode materials along with increasing the MEC current density operation.

Fig. 9 shows the detailed production cost breakdown of an integrated DF-MEC facility producing 50 MT day^{-1} H_2 from SFW in various scenarios with different sources of electricity supply, CO_2 byproduct utilization methods, and types of potential PTC applied, based on the GHG emissions for each case shown in Fig. 4. Similar to the CW-fed case, each aforementioned scenario is compared based on MEC operating current densities of 20 A m^{-2}, 50 A m^{-2} and 100 A m^{-2}. The bioH_2 production costs vary between \$5.0 kg^{-1} and \$31 kg^{-1}, including \$2.9 kg^{-1} revenue earned in the form of net tipping fees. However, the consumption of electricity, KOH, and nutrients contributed \$3 to the production cost per kg of H_2 produced. This value is lower than those in the CW scenario because the amount of nutrients required in the CW scenario is higher than that in the SFW scenario. As mentioned earlier, bioH_2 production cost from SFW, operating at an MEC current density of 20 A m^{-2}, is not at all economically viable. The average production cost is \$30 kg^{-1} H_2, considering all the five cases assumed, as illustrated in Fig. 9.

We obtained production costs of \$10.6 (at 50 A m^{-2}) and \$5.7 (at 100 A m^{-2}) per kg H_2 with wind/solar as the electricity resource, revenues generated from tipping fees, CO_2 being sold to the beverage industry, and potential PTC obtained through 2022 IRA H_2 (45 V) for the first 10 years (second scenario of Fig. 9). The lowest H_2 production cost of \$5.0 kg^{-1} is achieved when using wind/solar electricity with CCS technology, with MEC operating at 100 A m^{-2}. The life cycle GHG emissions for this case are −8.00 kg per kg H_2, qualifying the system to obtain a PTC of \$3 kg^{-1} H_2 through the 2022 IRA H_2 (45 V).

Fig. 10 depicts the sensitivity of the cost of H_2 production using SFW as feedstock to different process parameters. The variations in the MEC current density exhibited the greatest impact on the fluctuations in H_2 production cost, followed by the IRR and H_2 output. Varying the current density by ±20% changes the net H_2 production cost by around ∓20%, while varying the IRR and H_2 output by ±20% varies the net production cost by ±11% and ∓10%, respectively, when MEC is operating at 20 A m^{-2}, 50 A m^{-2} and 100 A m^{-2}. This shows that for both plants, the MEC current density plays a vital role in reducing the final bioH_2 production cost.

Overall, both processes are modeled using validated lab test results from the literature, which represent the latest scientific discovery, with potential improvement *via* fundamental science advancements, *e.g.*, bacterial genetic engineering, MEC electrode and membrane development. Meanwhile, for the scaling up of plant operation, the DF yield and MEC current density are affected by factors other than scientific elements, *e.g.*, feedstock inconsistency and presence of impurity, mass and heat transfer limitations and material fouling. Efficient engineering design (*e.g.*, pretreatment to remove solids or impurities) and material/equipment development (*e.g.*, efficient propeller and anti-fouling practices) allow efficient scaling with satisfactory yield towards commercialization.

Conclusions

This study investigated the economic and environmental prospects of two 50 MT day^{-1} bioH_2 production facilities using CW and SFW as feedstock and producing high-purity CO_2 as a byproduct. The CO_2 is either sold to the beverage industry or captured and sequestered. Since both feedstocks are waste streams, they can potentially contribute discharge/tipping revenue earning opportunities instead of being expenses. Discharge fees for the CW varied according to plant location because the COD and TSS rates varied with location. The discharge fees were \$5.6, \$6.3 and \$11.3 per kg H_2 produced for the midwestern, southern and western U.S. regions, respectively. The tipping fees for SFW were based on typical municipal solid waste fees and had a flat rate of \$53 MT^{-1} (ref. 116) across the U.S. A tipping fee of \$2.9 kg^{-1} H_2 can be regarded as revenue earned. Based on literature data (Table S4†), MEC operating at current density was set to 20 A m^{-2}, 50 A m^{-2} and 100 A m^{-2} to observe their impact on the final bioH_2 production costs for both feedstocks.

Economic analysis showed that the MEC section is the primary contributor to the installed capital cost, emphasizing the need for further research to increase the current density of MEC operation along with using cheaper electrode materials. These observations are further supported in the bioH_2 cost sensitivity analysis plots of CW and SFW scenarios. In the CW scenario, the discharge fee significantly affected the final production cost of bioH_2, demonstrating a \$5-\$11 kg^{-1} cost reduction, and it was observed that with an increase in current density from 20 A m^{-2} to 100 A m^{-2}, the discharge fee was the most sensitive parameter.

Since the waste streams do not carry emissions burdens from upstream, the life cycle GHG emissions of bioH_2 production depend only on the carbon intensities of electricity and nutrients. Using renewable electricity together with CCS technology, the bioH_2 produced from both feedstocks is carbon negative, qualifying the system to receive a PTC of \$3 kg^{-1} H_2 under 2022 IRA 45 V. For both feedstocks, 45 V leads to greater benefits (about \$2.1 kg^{-1} reduction over the life of the project) than 45 Q (about \$0.4 kg^{-1} reduction). However, the wastewater discharge exhibits the highest benefit (\$5-\$11 kg^{-1} cost reduction).

The study further quantified WCF, which is a cost to most plants using process water. Both plants assessed in this work have no water consumption since they used the organic matter of the waste streams to produce H_2 and gave away clean water, some of which is reutilized by the process, thereby eliminating the need to buy process water from outside. An average of 23 and 21 gallons of clean water per kg bioH_2 was produced and/or discharged through DF-MEC of CW and SFW, respectively, unlike H_2 production methods, such as SMR and PEM electrolysis, which consume fresh water.[6]

This study showed the potential of low-cost H_2 production pathways using DF-MEC integration, different electricity sources and CO_2 utilization/sequestration strategies. For the two waste feedstocks, the MEC process needs further research

and development to increase the current density and further reduce the total capital costs. From a low-cost bioH_2 production viewpoint, all CW-fed scenarios showed significant potential across all three U.S. regions evaluated, especially the western region, considering current densities of 50 and 100 A m^{-2}. However, none of the scenarios are economically feasible with MEC operating at a current density of 20 A m^{-2}. Some of the limitations of this study are the variable composition of the waste feedstock, especially solid food waste, and the maintenance costs and lifetime operational hours of the MEC.

BioH_2 production is more capital intensive than PEM electrolysis owing to the lower current density of MEC, which requires further research. However, bioH_2 production from waste streams has advantages in lower electricity consumption (20–22 kW h kg^{-1} H_2 *vs.* 55 kW h kg^{-1} H_2 from PEM[7]) and the generation of treated clean water instead of consuming fresh water. This makes bioH_2 production extremely attractive in areas with a constrained water supply and a high wastewater discharge fee, such as California.

Author contributions

Conceptualization of idea: P. S., A. E., and A. G.; methodology: A. G., P. S., H. D., and X. L.; investigation of analysis: A. G. and P. S.; writing the manuscript: A. G.; reviewing and editing the manuscript: P. S., A. E., A. G., X. L., H. D., and L. S.; supervision and funding acquisition: P. S. and A. E.

Data availability

The contributions of this study are included in the main article and ESI.† Further data are available upon request.

Conflicts of interest

There are no conflicts to declare.

Acknowledgements

This research effort was supported by the Hydrogen and Fuel Cell Technologies Office of the U.S. Department of Energy's Office of Energy Efficiency and Renewable Energy under Contract Number DE-AC02-06CH11357. The views and opinions of the authors expressed herein do not necessarily state or reflect those of the United States Government or any agency thereof. Neither the United States Government nor any agency thereof, nor any of their employees, makes any warranty, expressed or implied, or assumes any legal liability or responsibility for the accuracy, completeness, or usefulness of any information, apparatus, product, or process disclosed, or represents that its use would not infringe privately owned rights.

References

1 R. Jackson, The Effects of Climate Change, **https://climate.nasa.gov/effects**, (accessed February 1, 2024).
2 U.S. Energy, Information Administration - EIA - Independent Statistics and Analysis, **https://www.eia.gov/consumption/manufacturing/data/2018/**, (accessed February 1, 2024).
3 Study Shows Abundant Opportunities for Hydrogen in a Future Integrated Energy System, **https://www.nrel.gov/news/program/2020/study-shows-abundant-opportunities-for-hydrogen-in-a-future-integrated-energy-system.html**, (accessed February 1, 2024).
4 F. Joseck, T. Nguyen, B. Klahr and A. Talapatra, *Current U. S. Hydrogen Production*, 2016.
5 M. Ruth, P. Jadun, N. Gilroy, E. Connelly, R. Boardman, A. J. Simon, A. Elgowainy and J. Zuboy, *The Technical and Economic Potential of the H2@Scale Hydrogen Concept within the United States*, 2020.
6 M. Wang, A. Elgowainy, U. Lee, K. H. Baek, A. Bafana, P. T. Benavides, A. Burnham, H. Cai, V. Cappello, P. Chen, Y. Gan, U. R. Gracida-Alvarez, T. R. Hawkins, R. K. Iyer, J. C. Kelly, T. Kim, S. Kumar, H. Kwon, K. Lee, X. Liu, Z. Lu, F. H. Masum, C. Ng, L. Ou, K. Reddi, N. Siddique, P. Sun, P. Vyawahare, H. Xu and G. G. Zaimes, *Summary of Expansions and Updates in GREET® 2022*, Argonne National Laboratory (ANL), Argonne, IL (United States), 2022.
7 B. D. James, D. A. DeSantis and G. Saur, *Final Report: Hydrogen Production Pathways Cost Analysis (2013–2016)*, Strategic Analysis Inc., Arlington, VA (United States), 2016.
8 Wastewater Infrastructure, **https://www.energy.gov/scep/slsc/wastewater-infrastructure**, (accessed February 1, 2024).
9 Y. Shen, J. L. Linville, M. Urgun-Demirtas, M. M. Mintz and S. W. Snyder, *Renewable Sustainable Energy Rev.*, 2015, **50**, 346–362.
10 Executive summary – Global Hydrogen Review 2021 – Analysis, **https://www.iea.org/reports/global-hydrogen-review-2021/executive-summary**, (accessed May 10, 2024).
11 W. Williams-Derry, *IEEFA U.S.*: *Booming U.S. natural gas exports fuel high prices*, 2021.
12 R. D. Cusick, P. D. Kiely and B. E. Logan, *Int. J. Hydrogen Energy*, 2010, **35**, 8855–8861.
13 S. Vijaya Krishna, P. Kiran Kumar, N. Chaitanya, D. Bhagawan, V. Himabindu and M. Lakshmi Narasu, *Biofuels*, 2017, **8**, 701–707.
14 R. Moreno, A. Escapa, J. Cara, B. Carracedo and X. Gómez, *Int. J. Hydrogen Energy*, 2015, **40**, 168–175.
15 Cheese Industry Profile, **https://www.agmrc.org/commodities-products/livestock-dairy-poultry/dairy/cheese-industry-profile**, (accessed February 1, 2024).
16 A. R. Prazeres, S. Luz, F. Fernandes and E. Jerónimo, *J. Environ. Chem. Eng.*, 2020, **8**, 103556.
17 A. R. Prazeres, F. Carvalho and J. Rivas, *J. Environ. Manage.*, 2012, **110**, 48–68.

18 O. US EPA, From Field to Bin, **https://www.epa.gov/land-research/field-bin-environmental-impacts-us-food-waste-management-pathways**, (accessed February 1, 2024).
19 O. US EPA, National Overview, **https://www.epa.gov/facts-and-figures-about-materials-waste-and-recycling/national-overview-facts-and-figures-materials**, (accessed February 1, 2024).
20 L. Bhatia, H. Jha, T. Sarkar and P. K. Sarangi, *Int. J. Environ. Res. Public Health*, 2023, **20**, 2318.
21 S. E. Hosseini and M. A. Wahid, *Renewable Sustainable Energy Rev.*, 2016, **57**, 850–866.
22 C. A. García, R. Betancourt and C. A. Cardona, *J. Environ. Manage.*, 2017, **203**, 695–703.
23 S. Jia, S. Ning, H. Ying, Y. Sun, W. Xu and H. Yin, *Energy Convers. Manage.*, 2017, **151**, 457–464.
24 I. Adánez-Rubio, F. García-Labiano, A. Abad, L. F. De Diego and J. Adánez, *Chem. Eng. J.*, 2022, **431**, 133376.
25 A. Arregi, G. Lopez, M. Amutio, I. Barbarias, J. Bilbao and M. Olazar, *RSC Adv.*, 2016, **6**, 25975–25985.
26 P. Nikolaidis and A. Poullikkas, *Renewable Sustainable Energy Rev.*, 2017, **67**, 597–611.
27 V. Singh and D. Das, in *Science and Engineering of Hydrogen-Based Energy Technologies*, ed. P. E. V. de Miranda, Academic Press, 2019, pp. 123–164.
28 M. Kim, J. Baek, Y. Yun, S. Junsim, S. Park and S. Kim, *Int. J. Hydrogen Energy*, 2006, **31**, 812–816.
29 R. Łukajtis, I. Hołowacz, K. Kucharska, M. Glinka, P. Rybarczyk, A. Przyjazny and M. Kamiński, *Renewable Sustainable Energy Rev.*, 2018, **91**, 665–694.
30 G. Kumar, S. Shobana, D. Nagarajan, D.-J. Lee, K.-S. Lee, C.-Y. Lin, C.-Y. Chen and J.-S. Chang, *Curr. Opin. Biotechnol.*, 2018, **50**, 136–145.
31 M.-L. Chong, V. Sabaratnam, Y. Shirai and M. A. Hassan, *Int. J. Hydrogen Energy*, 2009, **34**, 3277–3287.
32 H. Liu, N. Agrawal, A. Ganguly, Y. Chen, J. Lee, J. Yu, W. Huang, M. Mba Wright, M. J. Janik and W. Li, *Energy Environ. Sci.*, 2022, **15**, 4175–4189.
33 P. Dange, A. Kumar, N. Savla, S. Khilari, S. Dutta, P. K. Gupta, K. K. Pandey, A. S. Mathuriya, Kanupriya, S. Agarwal and S. Pandit, in *Innovations in Fermentation and Phytopharmaceutical Technologies*, ed. H. Thatoi, S. Mohapatra and S. K. Das, Elsevier, 2022, pp. 221–244.
34 W. Xu, C. Yu, J. Chen and Z. Liu, *Appl. Catal., B*, 2022, **305**, 121062.
35 J. P. Polin, C. A. Peterson, L. E. Whitmer, R. G. Smith and R. C. Brown, *Appl. Energy*, 2019, **249**, 276–285.
36 C. Putatunda, M. Behl, P. Solanki, S. Sharma, S. K. Bhatia, A. Walia and R. K. Bhatia, *Int. J. Hydrogen Energy*, 2023, **48**, 21088–21109.
37 B. Senthil Rathi, P. Senthil Kumar, G. Rangasamy and S. Rajendran, *Int. J. Hydrogen Energy*, 2024, **52**, 115–138.
38 M. Karimi Alavijeh, S. Yaghmaei and M. M. Mardanpour, *Bioenergy Res.*, 2020, **13**, 463–476.
39 T. Zhang, D. Jiang, H. Zhang, Y. Jing, N. Tahir, Y. Zhang and Q. Zhang, *Int. J. Hydrogen Energy*, 2020, **45**, 3807–3814.
40 G. Balachandar, N. Khanna and D. Das, in *Biohydrogen*, ed. A. Pandey, J.-S. Chang, P. C. Hallenbecka and C. Larroche, Elsevier, Amsterdam, 2013, pp. 103–144.
41 T. Weide, E. Brügging, C. Wetter, A. Ierardi and M. Wichern, *Int. J. Hydrogen Energy*, 2019, **44**, 24110–24125.
42 B. Senthil Rathi, P. Senthil Kumar, G. Rangasamy and S. Rajendran, *Int. J. Hydrogen Energy*, 2024, **52**, 115–138.
43 A. Ahmad, R. K, S. W. Hasan, P. L. Show and F. Banat, *Int. J. Hydrogen Energy*, 2024, **52**, 335–357.
44 X. Qu, H. Zeng, Y. Gao, T. Mo and Y. Li, *Front. Chem.*, 2022, **10**, DOI: **10.3389/fchem.2022.978907**.
45 Dark Fermentation - an overview|ScienceDirect Topics, **https://www.sciencedirect.com/topics/engineering/dark-fermentation**, (accessed May 10, 2024).
46 S. Satyapal, *2017 Annual Progress Report: DOE Hydrogen and Fuel Cells Program*, National Renewable Energy Lab. (NREL), Golden, CO (United States), 2018.
47 A. Hosseinzadeh, J. L. Zhou, X. Li, M. Afsari and A. Altaee, *Renewable Sustainable Energy Rev.*, 2022, **156**, 111991.
48 W. Han, Y. Y. Hu, S. Y. Li, F. F. Li and J. H. Tang, *Bioresour. Technol.*, 2016, **221**, 318–323.
49 J.-Y. Lee, Y.-B. Sim, J.-H. Jung, A. K. Pandey, D. Kyung and S.-H. Kim, *Energy*, 2024, **312**, 133559.
50 R. Yukesh Kannah, S. Kavitha, Preethi, O. Parthiba Karthikeyan, G. Kumar, N. V. Dai-Viet and J. Rajesh Banu, *Bioresour. Technol.*, 2021, **319**, 124175.
51 A. Kadier, Y. Simayi, M. S. Kalil, P. Abdeshahian and A. A. Hamid, *Renewable Energy*, 2014, **71**, 466–472.
52 A. Escapa, M. I. San-Martín and A. Morán, *Front. Energy Res.*, 2014, **2**, DOI: **10.3389/fenrg.2014.00019**.
53 A. Segundo-Aguilar, L. V. González-Gutiérrez, V. C. Payá, J. Feliu, G. Buitrón and B. Cercado, *Sustainable Energy Fuels*, 2021, **5**, 2003–2017.
54 J. Chen, W. Xu, X. Wu, J. E, N. Lu, T. Wang and H. Zuo, *Energy Convers. Manage.*, 2019, **193**, 52–63.
55 A. Verma and A. Kumar, *Appl. Energy*, 2015, **147**, 556–568.
56 M. Cerrillo, M. Viñas and A. Bonmatí, *Bioresour. Technol.*, 2016, **216**, 362–372.
57 K. P. Katuri, C. M. Werner, R. J. Jimenez-Sandoval, W. Chen, S. Jeon, B. E. Logan, Z. Lai, G. L. Amy and P. E. Saikaly, *Environ. Sci. Technol.*, 2014, **48**, 12833–12841.
58 Y. Chen, M. Chen, N. Shen and R. J. Zeng, *Int. J. Hydrogen Energy*, 2016, **41**, 22760–22768.
59 A. Wang, D. Sun, G. Cao, H. Wang, N. Ren, W.-M. Wu and B. E. Logan, *Bioresour. Technol.*, 2011, **102**, 4137–4143.
60 Y. Koul, V. Devda, S. Varjani, W. Guo, H. H. Ngo, M. J. Taherzadeh, J.-S. Chang, J. W. C. Wong, M. Bilal, S.-H. Kim, X.-T. Bui and R. Parra-Saldívar, *Bioengineered*, 2022, **13**, 8115–8134.
61 A. Marone, O. R. Ayala-Campos, E. Trably, A. A. Carmona-Martínez, R. Moscoviz, E. Latrille, J.-P. Steyer, V. Alcaraz-Gonzalez and N. Bernet, *Int. J. Hydrogen Energy*, 2017, **42**, 1609–1621.
62 X.-H. Li, D.-W. Liang, Y.-X. Bai, Y.-T. Fan and H.-W. Hou, *Int. J. Hydrogen Energy*, 2014, **39**, 8977–8982.

63 N. Azbar, F. T. Çetinkaya Dokgöz, T. Keskin, K. S. Korkmaz and H. M. Syed, *Int. J. Hydrogen Energy*, 2009, **34**, 7441–7447.
64 R. E. Davis, N. J. Grundl, L. Tao, M. J. Biddy, E. C. Tan, G. T. Beckham, D. Humbird, D. N. Thompson and M. S. Roni, *Process Design and Economics for the Conversion of Lignocellulosic Biomass to Hydrocarbon Fuels and Coproducts: 2018 Biochemical Design Case Update; Biochemical Deconstruction and Conversion of Biomass to Fuels and Products via Integrated Biorefinery Pathways*, National Renewable Energy Lab. (NREL), Golden, CO (United States), 2018.
65 R. D. Doctor, J. C. Molburg and P. R. Thimmapuram, *KRW oxygen-blown gasification combined cycle: Carbon dioxide recovery, transport, and disposal*, 1996.
66 J. C. Minge, G. L. Armstrong, J. L. Nichols, M. W. Nichols, *MEETING THE DUAL CHALLENGE; A Roadmap to At-Scale Deployment of CARBON CAPTURE, USE, AND STORAGE; Chapter Six - CO2 Transport*, National Petroleum Council, 2019.
67 S.-H. Kim and H.-S. Shin, *Int. J. Hydrogen Energy*, 2008, **33**, 5266–5274.
68 B. James, W. Colella, J. Moton, G. Saur and T. Ramsden, *PEM Electrolysis H2A Production Case Study Documentation*, 2013.
69 Aspen Plus|Leading Process Simulation Software| AspenTech, **https://www.aspentech.com/en/products/engineering/aspen-plus**, (accessed February 1, 2024).
70 R. Davis, M. J. Biddy, E. Tan, L. Tao and S. B. Jones, *Biological Conversion of Sugars to Hydrocarbons Technology Pathway*, Pacific Northwest National Lab. (PNNL), Richland, WA (United States), 2013.
71 D. Humbird, R. Davis, L. Tao, C. Kinchin, D. Hsu, A. Aden, P. Schoen, J. Lukas, B. Olthof, M. Worley, D. Sexton and D. Dudgeon, *Process Design and Economics for Biochemical Conversion of Lignocellulosic Biomass to Ethanol: Dilute-Acid Pretreatment and Enzymatic Hydrolysis of Corn Stover*, 2011.
72 A. T. Mayyas, M. F. Ruth, B. S. Pivovar, G. Bender and K. B. Wipke, *Manufacturing Cost Analysis for Proton Exchange Membrane Water Electrolyzers*, 2019.
73 A. Escapa, X. Gómez, B. Tartakovsky and A. Morán, *Int. J. Hydrogen Energy*, 2012, **37**, 18641–18653.
74 R. K. Goud, O. Sarkar, P. Chiranjeevi and S. Venkata Mohan, *Bioresour. Technol.*, 2014, **165**, 223–232.
75 J. D. Holladay, J. Hu, D. L. King and Y. Wang, *Catal. Today*, 2009, **139**, 244–260.
76 G. De Gioannis, M. Friargiu, E. Massi, A. Muntoni, A. Polettini, R. Pomi and D. Spiga, *Int. J. Hydrogen Energy*, 2014, **39**, 20930–20941.
77 Y. H. Seo, Y.-M. Yun, H. Lee and J.-I. Han, *Fuel*, 2015, **150**, 202–207.
78 P. R. F. Rosa, S. C. Santos, I. K. Sakamoto, M. B. A. Varesche and E. L. Silva, *Bioresour. Technol.*, 2014, **161**, 10–19.
79 E. François, C. Dumas, R. D. Gougeon, H. Alexandre, S. Vuilleumier and B. Ernst, *Bioresour. Technol.*, 2021, **320**, 124334.
80 G. Policastro, F. Carraturo, M. Compagnone, M. Guida and M. Fabbricino, *Bioresour. Technol. Rep.*, 2022, **19**, 101196.
81 P. Thanwised, W. Wirojanagud and A. Reungsang, *Int. J. Hydrogen Energy*, 2012, **37**, 15503–15510.
82 S. Marks, J. Dach, J. L. Garcia-Morales and F. J. Fernandez-Morales, *Appl. Sci.*, 2020, **10**, 8360.
83 Integration of Dark Fermentation with Microbial Electrolysis Cells for Biohydrogen and Methane Production from Distillery Wastewater and Glycerol Waste Co-Digestion, **https://www.mdpi.com/2311-5637/8/10/537**, (accessed February 17, 2025).
84 I. Z. Boboescu, M. Ilie, V. D. Gherman, I. Mirel, B. Pap, A. Negrea, É. Kondorosi, T. Bíró and G. Maróti, *Biotechnol. Biofuels*, 2014, **7**, 139.
85 C.-H. Lay, B. Sen, S.-C. Huang, C.-C. Chen and C.-Y. Lin, *Renewable Energy*, 2013, **58**, 60–67.
86 R. Davis, L. Tao, C. Scarlata, E. C. D. Tan, J. Ross, J. Lukas and D. Sexton, *Process Design and Economics for the Conversion of Lignocellulosic Biomass to Hydrocarbons: Dilute-Acid and Enzymatic Deconstruction of Biomass to Sugars and Catalytic Conversion of Sugars to Hydrocarbons*, National Renewable Energy Lab. (NREL), Golden, CO (United States), 2015.
87 W. Liu, S. Huang, A. Zhou, G. Zhou, N. Ren, A. Wang and G. Zhuang, *Int. J. Hydrogen Energy*, 2012, **37**, 13859–13864.
88 S. Agnihotri, D.-M. Yin, A. Mahboubi, T. Sapmaz, S. Varjani, W. Qiao, D. Y. Koseoglu-Imer and M. J. Taherzadeh, *Bioengineered*, 2022, **13**, 1249–1275.
89 P. Spath, A. Aden, T. Eggeman, M. Ringer, B. Wallace and J. Jechura, *Biomass to Hydrogen Production Detailed Design and Economics Utilizing the Battelle Columbus Laboratory Indirectly-Heated Gasifier*, National Renewable Energy Lab. (NREL), Golden, CO (United States), 2005.
90 ISO 14040, **https://www.iso.org/standard/37456.html**, (accessed February 17, 2025).
91 ISO 14044, **https://www.iso.org/standard/38498.html**, (accessed February 17, 2025).
92 GREET, **https://www.energy.gov/eere/greet**, (accessed February 1, 2024).
93 Clean Hydrogen Production Tax Credit (45 V) Resources, **https://www.energy.gov/articles/clean-hydrogen-production-tax-credit-45v-resources**, (accessed February 1, 2024).
94 DOE Loan Guarantees & IRS Guidance on 45Q Tax Credit Could Benefit Carbon Capture Projects, **https://www.energy.gov/lpo/articles/doe-loan-guarantees-irs-guidance-45q-tax-credit-could-benefit-carbon-capture-projects**, (accessed February 1, 2024).
95 Aspen Process Economic Analyzer, **https://www.aspentech.com/en/products/engineering/aspen-process-economic-analyzer**, (accessed February 1, 2024).
96 A. W. Jeremiasse, H. V. M. Hamelers, M. Saakes and C. J. N. Buisman, *Int. J. Hydrogen Energy*, 2010, **35**, 12716–12723.
97 A. G. Miller, *Microbial Electrolysis Cells for the Production of Hydrogen Gas: Evaluation of Internal Resistance and Design for Scale-Up*, Oregon State University, 2018.

98 H. Liu, *Novel Hybrid Microbial Electrochemical System for Efficient Hydrogen Generation from Biomass (Project ID PD129)*, 2018.
99 K. Harrison, *MW-Scale PEM-Based Electrolyzers for RES Applications (CRADA CRD-18-00742 Final Report)*, National Renewable Energy Lab. (NREL), Golden, CO (United States), 2021.
100 T. Brinkmann, S. G. Giner, F. Schorcht, S. Roudier and S. L. Delgado, Best Available Techniques (BAT) Reference Document for the Production of Chlor-alkali. Industrial Emissions Directive 2010/75/EU (Integrated Pollution Prevention and Control), **https://publications.jrc.ec.europa.eu/repository/handle/JRC91156**, (accessed May 14, 2024).
101 Track Caustic Potash price trend and forecast in top 10 leading countried worldwide, accessed January 2024, **https://www.chemanalyst.com/Pricing-data/caustic-potash-1212**.
102 White Crystalline Granular Kcl Chloride Potassium 99% Powder Chemical Grade from Charity Chemicals Inc, **https://www.echemi.com/produce/pr2303179642-white-crystalline-granular-kcl-chloride-potassium-99-powder.html**, (accessed February 1, 2024).
103 FCC Dipotassium Phosphate, **https://www.echemi.com/produce/pr2312111268-fcc-dipotassium-phosphate.html**, (accessed February 1, 2024).
104 High Quality Ammonium Chloride Salmiac NH_4CL Ammonium Chloride Powder CAS 12125-02-9 Industrial Grade, **https://www.echemi.com/produce/pr2308071181-high-quality-ammonium-chloride-salmiac-nh4cl-ammonium-chloride-powder-cas-12125-02-9.html**, (accessed February 1, 2024).
105 Magnesium Fertilizer Industrial Grade Magnesium Sulfate Heptahydrate Industrial Grade, **https://www.echemi.com/produce/pr2308051009-factory-prices-magnesium-fertilizer-industrial-grade-magnesium-sulfate-heptahydrate.html**, (accessed February 1, 2024).
106 Copper(II) chloride Industrial Grade, **https://www.echemi.com/produce/pr2305111434-copperii-chloride.html**, (accessed February 1, 2024).
107 Buy $ZnCl_2$ battery grade Zinc Chloride 99% factory price/cas, **https://www.echemi.com/produce/pr2303272342-zncl2-battery-grade-zinc-chloride-99-factory-price-cas7646-85-7.html**, (accessed February 1, 2024).
108 Boric acid cas 11113-50-1 boric acid 99% White Powder BH_3O_3 Industrial Grade, **https://www.echemi.com/produce/pr2305161749-supply-hot-product-boric-acid-cas-11113-50-1-boric-acid-99-white-powder-bh3o3.html**, (accessed February 1, 2024).
109 Manganese chloride tetrahydrate cas 13446-34-9 best price mncl2 manganous chloride Industrial Grade, **https://www.echemi.com/produce/pr2303293298-factory-hot-selling-manganese-chloride-tetrahydrate-cas-13446-34-9-best-price-mncl2-manganous-chloride.html**, (accessed February 1, 2024).
110 High quality Ferrous chloride tetrahydrate CAS 13478-10-9 99% blue-green crystal, **https://www.echemi.com/produce/pr2303294259-high-quality-ferrous-chloride-tetrahydrate-cas-13478-10-9-99-blue-green-crystal-hjz-hjz.html**, (accessed February 1, 2024).
111 Ammonium molybdate tetrahydrate, Industrial Grade, **https://www.echemi.com/searchGoods/pd180521115655-ammonium-molybdate-tetrahydrate.html**, (accessed February 1, 2024).
112 Cobalt(II) chloride hexahydrate Industrial Grade, **https://www.echemi.com/produce/pr2204292905-cobaltii-chloride-hexahydrate.html**, (accessed February 1, 2024).
113 Nickel chloride 98% Cas No. 7791-20-0 Industrial Grade, **https://www.echemi.com/produce/pr2108041032-nickel-chloride-98-cas-no-7791-20-0.html**, (accessed February 1, 2024).
114 A. Ganguly, R. C. Brown and M. M. Wright, *Green Chem.*, 2022, **24**, 9290–9302.
115 The Physical CO_2 Market, **https://dotyenergy.com/Economics/Econ_Physical_CO2_Market.htm**, (accessed February 1, 2024).
116 U.S. landfill dump fees by region 2022, **https://www.statista.com/statistics/692063/cost-to-landfill-municipal-solid-waste-by-us-region/**, (accessed February 1, 2024).
117 Metropolitan Council, Industrial Waste Rates and Fees, **https://metrocouncil.org/Wastewater-Water/Services/Industrial-Waste/Industrial-Waste-Rates-Fees.aspx**.
118 Special Services: Selected Austin Water Utility Rates & Fees, **https://www.austintexas.gov/department/special-services-selected-austin-water-utility-rates-fees**.
119 HF&H Consultants, LLC, *UNION SANITARY DISTRICT WASTEWATER RATE AND COST OF SERVICE STUDY*, 2020.
120 A. Elgowainy, presented in part at the PRESENTATION AT DOE'S ELECTROLYZER INSTALLATION WORKSHOP, U.S. Depatment of Energy Electrolyzer Installation Workshop, 9/26, 2023.
121 R. K. Iyer, J. C. Kelly and A. Elgowainy, *Electrolyzers for Hydrogen Production: Solid Oxide, Alkaline, and Proton Exchange Membrane*, Argonne National Lab. (ANL), Argonne, IL (United States), 2022.